^{130}Te($\vec{p}$,p_1) and ^{130}Te(p,$\vec{p}_1$) reactions on analog resonances

J. L. Foster, Jr.,* S. E. Darden, M. C. Rozak, and J. A. Ross
Department of Physics, University of Notre Dame, Notre Dame, Indiana 46556

J. P. Martin, L. Lessard, S. Gales,† G. Noury, J. M. Pearson, and P. Depommier
Universite de Montreal, Montreal, Quebec, Canada

M. C. Hermida M. Ruiz
Instituto de Fisica, Universidade de São Paulo, São Paulo, Brazil
(Received 26 March 1984)

Elastic and inelastic proton scattering angular distributions of cross section and analyzing power were measured on three analog resonances at 10.30, 10.54, and 10.60 MeV in the ^{130}Te-plus-proton system. The data have been analyzed using a coupled-channels-plus-resonance formalism. Optical-model parameters required for the analysis were obtained from measurements at two off-resonance energies. Polarization measurements carried out on two of these resonances are consistent with values predicted from the analysis of the cross-section and analyzing-power data. The analysis yields improved values of the spectroscopic amplitudes for coupling of nucleons to the ^{130}Te 2_1^+ core.

I. INTRODUCTION

The usefulness of inelastic scattering measurements carried out on isobaric analog resonances (IAR's) as a means of obtaining spectroscopic amplitudes for comparison with nuclear-structure calculations has been recognized for more than a decade, and a number of such experiments have been reported in the literature.[1–11] An analysis[12] has recently been completed for coupling to the 2_1^+ core of ^{130}Te for six states in ^{131}Te, based on proton inelastic scattering cross-section measurements on the analogs of these states. The analysis employed combined Breit-Wigner resonance and coupled-channel scattering matrices. When the IAR is below or near the neutron threshold, the cross section can be enhanced by coherent contributions from $T^<$ states mixing with the analog state. In such cases, extraction of spectroscopic information requires determination of polarization in the exit channel, either directly, through double scattering measurements, or indirectly, through (p,p'γ) measurements.[8] The resonances in ^{130}Te(p,p_1) studied in Ref. 12 lie 7 to 10 MeV above the (p,n) threshold, so that cross-section and analyzing-power measurements should suffice for the extraction of spectroscopic information. In fact, this type of experiment offers the possibility of investigating couplings to more highly excited core states and of investigating the microscopic structure of the core states themselves.[13]

Although polarization measurements on the inelastically scattered protons may provide more detailed structure information than analyzing-power data, measurements with a polarized beam are still desirable, since the analyzing power is generally more sensitive to the contributions of different partial waves than is the cross section. It can be expected that a more precise determination of the different inelastic widths will be possible using both cross-section and analyzer-power data than is possible using cross-section data alone. General agreement with particle-vibrator coupling calculations gives some confidence in the results of these analyses, but an inherent problem is the description and determination of the direct part of the inelastic scattering amplitude. In this respect, a coupled-channels analysis of both cross-section and analyzing-power off-resonance data is of crucial importance.

In the work reported on here, angular distributions of cross section and analyzing power have been measured for three of the analog resonances in the ^{130}Te + p system studied in Ref. 12. In our analysis, spectroscopic amplitudes have been determined from cross-section data alone, from analyzing-power data alone, and from the combination of both kinds of data. The results are compared with those of Ref. 12. Our analysis differs significantly from that of Ref. 12 in that it employs an optical model whose parameters have been determined by fitting off-resonance data for both cross section and analyzing power, whereas in Ref. 12 only cross-section data were used. Polarization measurements on two of the resonances carried out using a silicon polarimeter are presented and compared with values predicted using the amplitudes resulting from the analysis of the cross-section and analyzing-power data.

II. EXPERIMENT

A. Cross-section and analyzing-power data

Cross sections and analyzing powers were measured using the polarized proton beam of the University of Notre Dame tandem accelerator. Data were taken at 10° intervals between 40° and 170° using an array of seven detectors. The beam polarization was determined and monitored from elastic scattering on the carbon backing and oxygen contamination of the Te (> 99% ^{130}Te) target using known analyzing powers.[14,15] Energy loss in the Te targets was about 5 keV. Off-resonance data were taken

at 9.5 and 14 MeV, and on-resonance measurements were made at 10.30, 10.54, and 10.60 MeV, corresponding to the analog resonances with spin-parity values $\frac{7}{2}^-$, $\frac{3}{2}^-$, and $\frac{3}{2}^-$, respectively.[12] Excitation functions of elastic cross section and analyzing power were also measured at six angles in 20–50 keV steps between 10.1 and 10.72 MeV. Absolute cross sections were determined by normalization to an optical model prediction at forward angles and off-resonance energies.

Results of the off-resonance measurements at 9.5 and 14 MeV are shown in Figs. 3 and 4. Elastic scattering excitation functions of cross section and analyzing power are given in Fig. 5, and the on-resonance measurements of elastic and inelastic scattering are presented in Figs. 6–8. The on-resonance data for the $\frac{7}{2}^-$ resonance shown in Fig. 6 were taken at the energy where the yield to the 2^+ state is a maximum. Energies for the on-resonance measurements on the $\frac{3}{2}^-$ levels were obtained from the energy spacings between the resonances given in Ref. 12. Analysis of the elastic-scattering data was used to accurately establish (± 1 keV) the value of the beam energies relative to the resonance energies. It is this difference which is of importance in the resonance analysis discussed below.

B. Polarization data

The polarization measurements were performed at the tandem laboratory of the University of Montreal with a double scattering polarimeter[16] which uses a silicon detector as the analyzer. This provides a means of measuring the energy loss in the analyzer, permitting the use of a rather thick analyzer without significant loss in energy resolution. The polarimeter is described in detail in Ref. 16. Protons scattered from the Si analyzer are detected in right and left detectors situated at back angles ($\pm 148°$) with respect to the analyzer. For these angles, the variation with angle of the ^{28}Si(p,p$_0$) analyzing power and cross section are not large, thus minimizing spurious asymmetries associated with small shifts in the position of the beam on the target. The slow variation with angle of $\sigma(\theta)$ and $A(\theta)$ near 148° also permits the use of rather large solid angles. For a given measurement, runs were taken on both sides of the incident proton beam to compensate for instrumental asymmetries associated with the electronics and solid angles. Finite geometry effects were determined to be only a small fraction of a percent and were not taken into account.

The effective analyzing power of the Si analyzer is a function of the threshold setting of the single-channel analyzers used with left and right proton detectors. These analyzers produce stop signals for the time-to-amplitude converters which provide a coincidence signal between the analyzer pulses and the proton detector pulses. Data were taken over a period of time in several runs using thresholds between 3.5 and 5.5 MeV. The effective analyzing power was interpolated from the curves shown in Fig. 1. In these measurements, the ^{130}Te targets were from 2 to 3 mg/cm^2 thick on a 10 μg/cm^2 carbon backing, corresponding to an energy loss in the targets of from 40 to 60 keV.[18] These targets could support up to 100 nA of beam without deterioration.

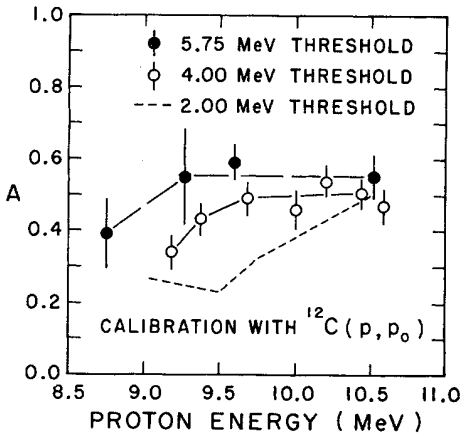

FIG. 1. Analyzing power of polarimeter for several thresholds on the proton detectors. The open circles are from Ref. 17, the dashed curve is from Ref. 14, and the solid circles are from the present work.

The upper portion of Fig. 2 shows a typical spectrum in the proton detectors. The lower part shows the same spectrum smoothed by taking a Fourier transform employing 512 sine and 512 cos terms, keeping ~120 of each, and transforming back to the original spectrum.[19] This procedure facilitated background subtraction and, we believe, resulted in a more precise determination of the peak areas. For every reaction peak in Fig. 2 there is a satellite peak from inelastic scattering to the 1.78 MeV state of ^{28}Si. The threshold setting in the proton detectors occurs at the extreme left end of the spectrum in Fig. 2. The energy resolution was about 150 keV. Results of the polarization measurements will be shown in Fig. 9. Uncertainties in center-of-target energies relative to the resonance energies are about ± 7 keV.

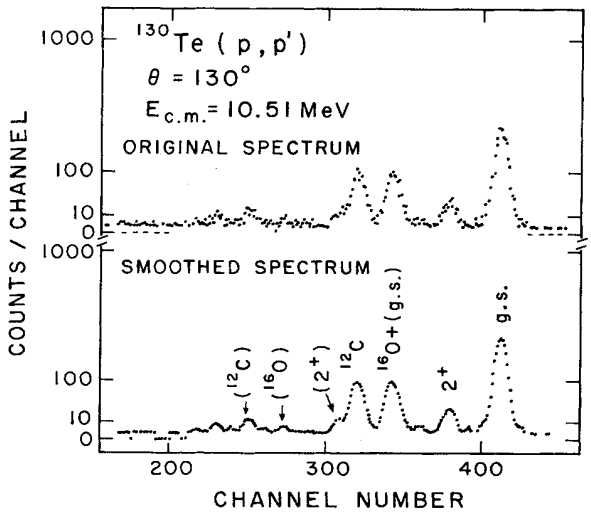

FIG. 2. Polarimeter spectrum. The upper part of the figure shows an unaltered spectrum; the lower part shows the same spectrum smoothed as described in the text.

III. ANALYSIS

The optical model potential used in the coupled-channels calculations was determined by simultaneously fitting both the elastic and inelastic scattering cross-section and analyzing-power data at 9.5 and 14.0 MeV. This analysis was done with the program ECIS 78 (Ref. 20) which has provision for a spin-orbit deformation and allows a different optical potential to be used for each channel. These provisions were not available in the program used in Ref. 12. Fits to the data resulting from this analysis are shown by the curves in Figs. 3 and 4. The optical potential parameters are given in Table I. Although the energies used, 9.5 and 14.0 MeV, are reasonably removed from the IAR's near 10.5 MeV, the effects of the tails of these resonances were taken into account in the analysis by adding to the optical model scattering matrices resonance scattering matrices as discussed below. The potential shapes used were the conventional ones and are the same as given in Ref. 12.

The coupled-channels optical potential given in Table I, which employs a deformation parameter for the imaginary potential of $\beta_I=0.08$, resulted in significantly improved fits to the on-resonance analyzing-power data, as compared with a potential having equal deformation parameters for the real and imaginary potentials. The use of different potentials for the ground and excited states requires some justification. Using more conventional parameters, we obtained less satisfactory fits to the off-resonance data. Since our goal in fitting these data is to obtain the best possible background amplitudes for use in the resonance analysis, we considered the use of the potential parameters of Table I to be preferable to forcing the parameters to conform to global values which result in a poorer fit to the off-resonance data.

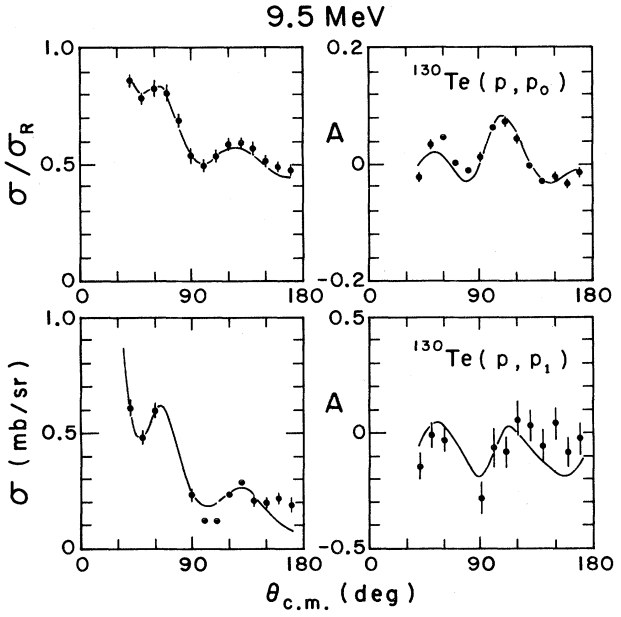

FIG. 3. Angular distributions of cross section and analyzing power for elastic and inelastic scattering of 9.5 MeV protons on ^{130}Te. The solid curves are coupled-channels optical model fits described in the text.

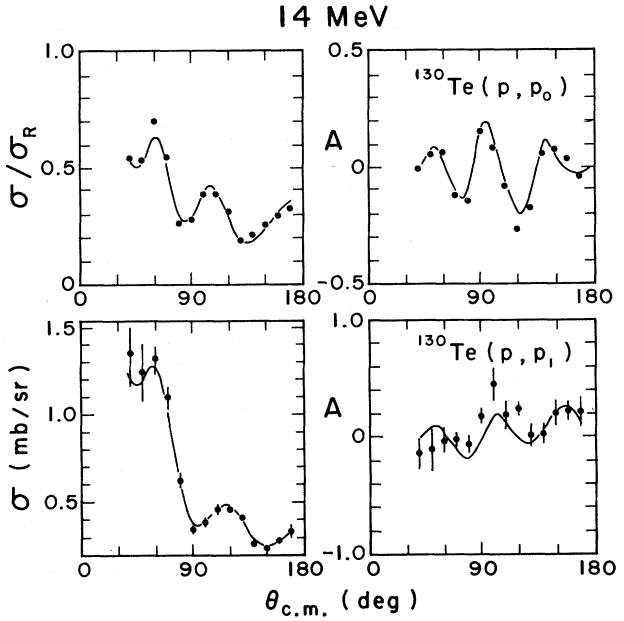

FIG. 4. Angular distributions of cross section and analyzing power for elastic and inelastic scattering of 14 MeV protons on ^{130}Te. The solid curves are coupled-channels optical model fits described in the text.

Figures 5 and 6 show fits to the elastic excitation-function data using the optical potential of Table I along with the resonance widths and phases of Ref. 12, but with shifts of a few keV in the IAR energies. The excellent quality of these fits confirms the spin-parity assignments of Ref. 12 and indicates that these parameters of the resonances were adequately determined by the cross-section data alone. There may be a small shift between the energy calibrations of the São Paulo and Notre Dame analyzing magnets. Somewhat wider slit openings were used on the energy analyzing magnet during the measurements with the polarized beam, and this may account for some of the discrepancy in resonance energies. It is also quite possible that by making small changes in the resonance phases, for example, the discrepancies could be removed. In view of the uncertainty regarding the origin of the discrepancies, we decided to allow the resonance energy to vary slightly, and keep the phases, total widths, and elastic widths as in Ref. 12.

The on-resonance angular distributions were fit using a modified version of ECIS 78 in which a resonant scattering matrix[21]

$$S^J_{\alpha\alpha'}=ie^{i(\phi_\alpha+\phi'_\alpha)}\sum_\lambda \frac{g(\alpha,J_\lambda)g(\alpha',J_\lambda)}{E_{J_\lambda}-E-\frac{i}{2}\Gamma_{J_\lambda}}$$

is added to a coupled-channels scattering matrix. Here $\alpha=(l,j,I_n)$ refers to the orbital angular momentum l and total spin j of a nucleon with respect to a core state I_n, E is the center of mass energy of the system, E_{J_λ} and Γ_{J_λ} are the energy and total width of the λth resonance with spin J, and $g(\alpha,J_\lambda)$ represents the square root of a partial width for the partition α for the resonance J_λ. The phase

TABLE I. Coupled-channels proton optical potential parameters for ^{130}Te. Subscripts R, I, SO, and C refer to real volume, surface imaginary, Thomas spin orbit, and Coulomb potentials, respectively. The β are the quadrupole potential deformation parameters; V and W are real and imaginary well depths, respectively.

r_R (fm)	r_I (fm)	r_{SO} (fm)	r_C (fm)	a_R (fm)	a_I (fm)	a_{SO} (fm)
1.25	1.27	1.03	1.25	0.686	0.652	0.400
Ground state	$V_R=$	61.97 MeV $-$	$(0.689)E_{lab}$			
	$W_I=$	8.53 MeV $+$	$(0.238)E_{lab}$			
2_1^+ state	$V_R=$	69.64 MeV $-$	$(1.176)E_{lab}$			
	$W_I=$	6.95 MeV $+$	$(0.300)E_{lab}$			
	$\beta_R=\beta_{SO}=$	$\beta_C=0.109$;	$\beta_I=0.08$			
	$V_{SO}=$	6.82 MeV				

ϕ_α is the sum of the resonance mixing phase, the Coulomb phase, and the real part of the optical phase.

In calculating the coupled-channels scattering matrix, partial waves up to $l=40$ were used. For $l\leq 15$ the sequential iteration technique of ECIS was used and the remaining partial waves were treated in an approximation using Coulomb wave functions.[22] For a given resonance, the square roots of the inelastic widths, the $g(\alpha',J_\lambda)$, were varied until a minimum χ^2 was reached. This was done in several steps, updating the values of $g(\alpha',J_\lambda)$ for other resonances while fitting data on a given resonance. The effect of the tail of the 11.02 MeV ($J^\pi=\frac{1}{2}^-$) IAR was included using the parameters of Ref. 12 for that resonance. Mixing phases, total widths, and elastic partial widths were taken from Ref. 12 and were not varied. Figures 7–9 show the best fits to the on-resonance angular distributions. The values of the $g(\alpha',J_\lambda)=g(ljI_n,J_\lambda)$ corresponding to these fits are presented in Table II.

Spectroscopic amplitudes defined as

$$\theta(l,j,I_n)=\frac{g(l,j,I_n,J_\lambda)}{g(l,j,I_n,J_\lambda)^{sp}}$$

were computed from the amplitudes of Table II. The single-particle amplitudes, $g(l,j,I_n,J_\lambda)^{sp}$, were calculated with program ANSPEC (Ref. 23) as

$$g(l,j,I_n,J_\lambda)^{sp}=h\frac{P_0(a_c)}{m_n a_c(2T_0+1)}u_n^{l,j,I_n}(a_c)\,,$$

where $u_n^{ljI_n}(a_c)$ is the value of the bound neutron wave function at radius a_c, m_n is the neutron mass, and $P_0(a_c)$ is the proton optical model penetrability. The single particle amplitudes are approximately constant over several Fermi at the nuclear surface. ANSPEC calculates $g(l,j,I_n,J_\lambda)$ for several radii near the nuclear surface, estimates the minimum value of $g(l,j,I_n,J_\lambda)$, and gives that minimum value as the single-particle amplitude.

Table III contains the spectroscopic amplitudes result-

TABLE II. Square roots of inelastic partial widths determined by fitting analyzing-power data, cross-section data, and both together with weight factors shown. Comparison with results of Ref. 12 is given.

Resonance laboratory energy (MeV) J^π	Cross section WT	Cross section χ^2	Analyzing power WT	Analyzing power χ^2	$g(p_{1/2},2^+)$	$g(p_{3/2},2^+)$	$g(f_{5/2},2^+)$	$g(f_{7/2},2^+)$
10.294	0	118	1	24		-0.0511	-0.0192	-0.0678
$\frac{7}{2}^-$	1	78	0	28		-0.0568	-0.0145	-0.0589
	1	80	2	26		-0.0548	-0.0130	-0.0614
		Ref. 12				-0.0623	-0.0115	-0.0485
10.540	0	7301	1	24	-0.0317	-0.0470	-0.0306	-0.0962
$\frac{3}{2}^-$	1	126	0	68	-0.0338	-0.0084	-0.0230	-0.0326
	1	138	2	42	-0.0261	-0.0161	-0.0203	-0.0385
		Ref. 12			-0.0344	-0.0051	-0.0090	-0.0451
10.609	0	605	1	9	-0.0300	-0.0500	-0.0095	-0.0618
$\frac{3}{2}^-$	1	321	0	25	-0.0513	-0.0422	$+0.0119$	-0.0660
	1	327	2	17	-0.0473	-0.0471	$+0.0109$	-0.672
		Ref. 12			-0.0572	-0.0596	-0.0108	-0.0705

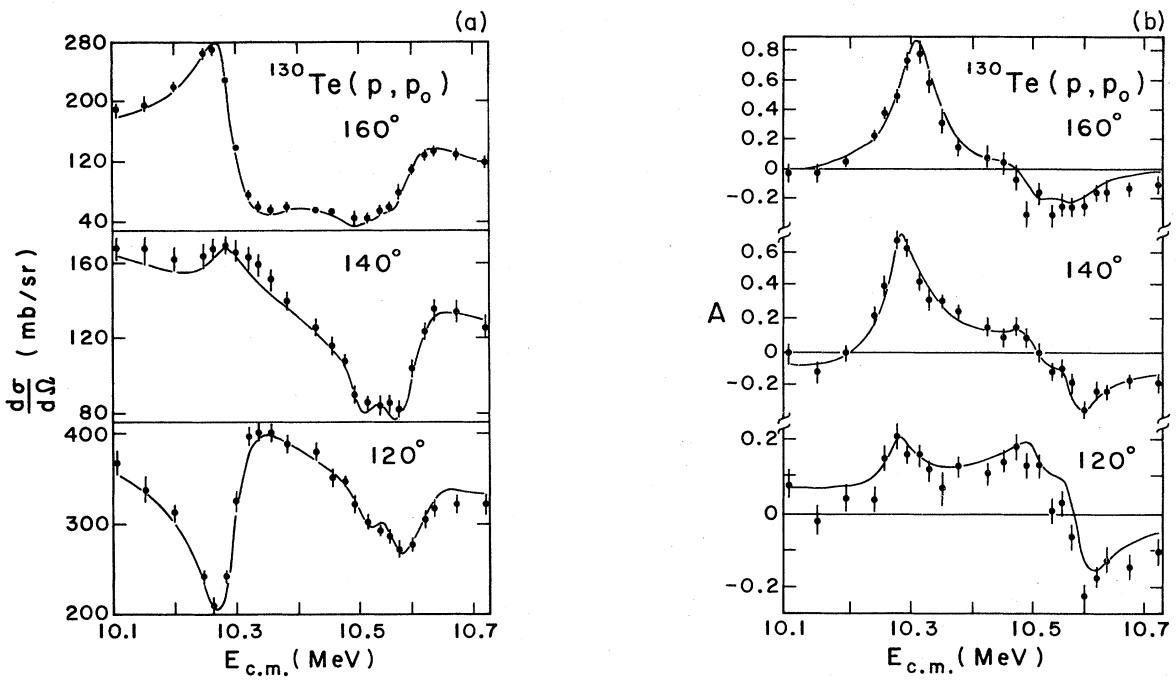

FIG. 5. Excitation functions of (a) cross section and (b) analyzing power for ^{130}Te(p,p_0). The curves show the fits to the data using partial elastic widths, total widths, and phases from Ref. 12.

ing from fits to the combined cross-section and analyzing-power data, those from the cross-section analysis of Ref. 12, and predictions of the quasiparticle vibrator calculations of Ref. 12.

Figure 9 shows a comparison of measured polarizations near the 10.30 MeV ($\frac{7}{2}^-$) and 10.60 MeV ($\frac{3}{2}^-$) resonances with polarizations calculated from the inelastic partial widths obtained fitting both cross-section and analyzing-

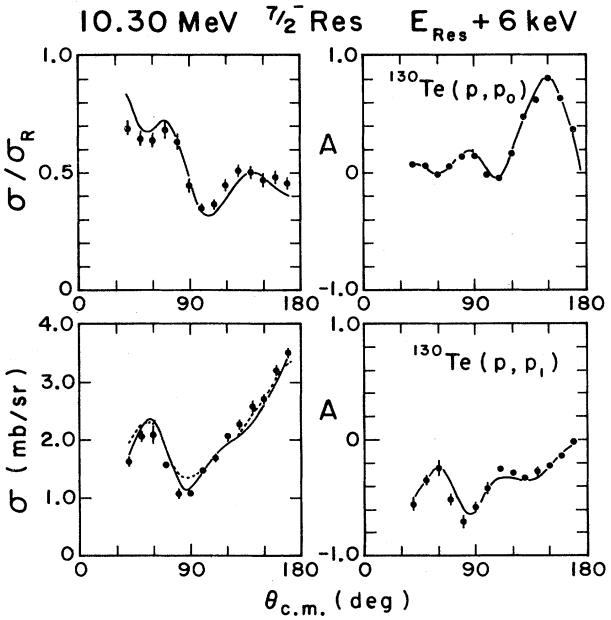

FIG. 6. On-resonance elastic and inelastic angular distributions of cross section and analyzing power for the $\frac{7}{2}^-$ resonance at 10.30 MeV. The solid curves are fits of both the cross-section and analyzing-power data. The dotted curve in the lower part of the figure shows the calculated cross section which results when a fit is made only to the analyzing-power data.

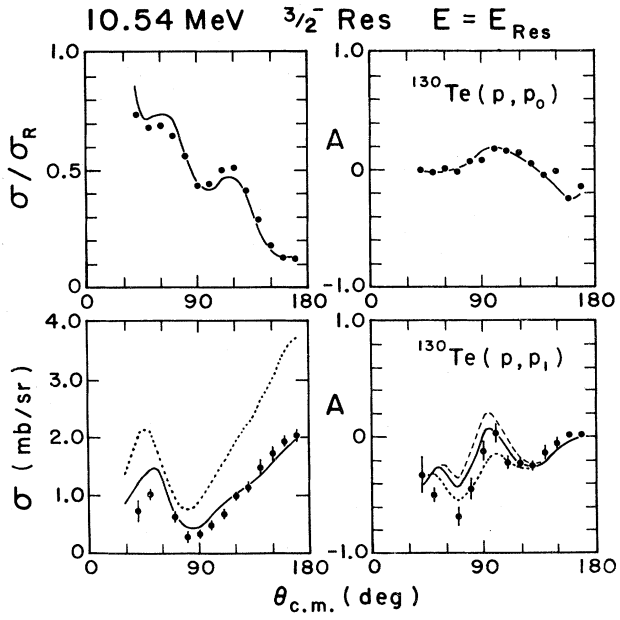

FIG. 7. On-resonance elastic and inelastic angular distributions of cross section and analyzing power for the $\frac{3}{2}^-$ resonance at 10.54 MeV. The solid curves are fits to both the cross-section and analyzing-power data. The dashed and dotted curves in the lower part of the figure correspond to fits to only the cross-section data and to only analyzing-power data, respectively.

TABLE III. Spectroscopic amplitudes from cross-section and analyzing-power data from present work ($X+A$), from Ref. 12 (experiment), and from Ref. 12 (theory).

Resonance laboratory energy	(MeV)	$\theta(l_j,0^+)$	$\theta(p_{1/2},2^+)$	$\theta(p_{3/2},2^+)$	$\theta(f_{5/2},2^+)$	$\theta(f_{7/2},2^+)$
10.294	$X+A$	0.77		−0.23	−0.09	−0.41
$\frac{7}{2}^-$	Ref. 12	0.76		−0.33	−0.09	−0.35
	Theory	0.67		−0.23	−0.04	−0.40
10.540	$X+A$	0.31	−0.12	−0.07	−0.09	−0.19
$\frac{3}{2}^-$	Ref. 12	0.32	−0.18	−0.03	−0.23	−0.31
	Theory	0.11	−0.03	−0.04	−0.14	−0.20
10.609	$X+A$	0.51	−0.21	−0.21	+0.07	−0.41
$\frac{3}{2}^-$	Ref. 12	0.53	−0.30	−0.39	−0.08	−0.47
	Theory	0.50	−0.15	−0.26	−0.08	−0.53

power data together with the total widths, elastic partial widths, and phases of Ref. 12.

IV. DISCUSSION

The results presented in Table II show that in most cases, fits to the cross-section data alone, to the analyzing-power data alone, or to the combined data, yield values of the inelastic partial widths which are not too different from each other. The partial widths from the present analysis are also generally consistent with those of Ref. 12, although in several cases there appear to be significant differences. Since the differences between widths resulting from analysis of cross-section data alone and widths resulting from analysis of the combined data are generally less than the differences between the present results and those of Ref. 12, it appears that these latter differences are mainly a consequence of the fact that different optical potentials were used in the two analyses. Also, the fact that the 10.54 MeV resonance was placed 9 keV further away from the 10.61 MeV resonance in the present analysis is probably responsible for the larger discrepancy with the results of Ref. 12 for this resonance. This change was required to fit the elastic angular distribution data for the 10.54 MeV resonance which are quite sensitive to the value of the resonance energy. The dotted curves in Figs. 6–8 show the calculated values of $\sigma(\theta)$ and $A(\theta)$ when only the analyzing-power data are fit. The differences between these curves and the solid curves are not very significant except in the case of the 10.54 MeV resonance. Whether or not this implies an inconsistency between the cross-section and analyzing-power data in this case is not clear. In any case, the most reliable widths would appear to be those obtained from analysis of the combined data. For the 10.54 MeV resonance somewhat larger uncertainties must be assigned.

The spectroscopic amplitudes obtained in the present

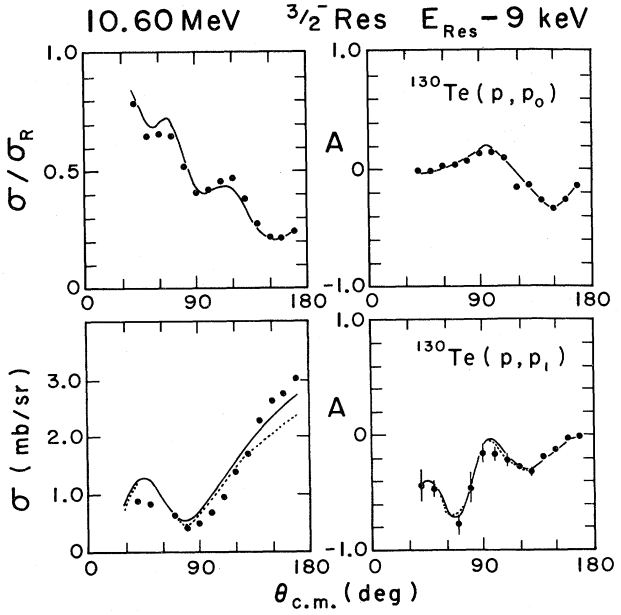

FIG. 8. On-resonance elastic and inelastic distributions of cross-section power and analyzing power for the $\frac{3}{2}^-$ resonance at 10.61 MeV. The description of the curves is as in Fig. 6.

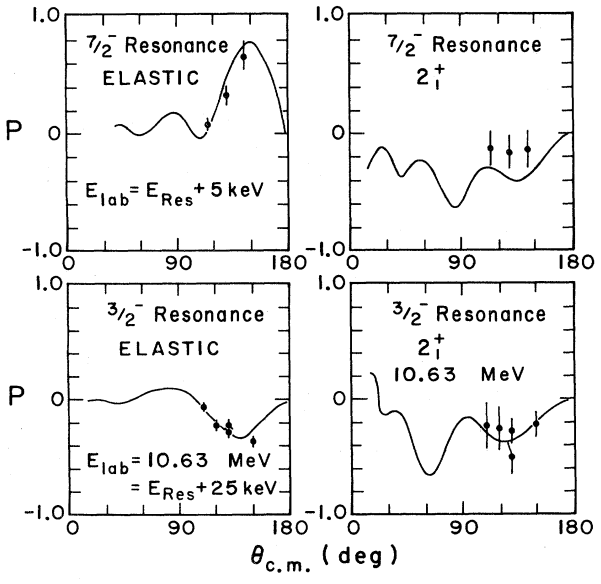

FIG. 9. Measured values of the polarization for ^{130}Te(p,p$_0$) and ^{130}Te(p,p$_1$) on the 10.30 and 10.60 MeV resonances. The curves were calculated using parameters resulting from the fits to the cross-section and analyzing power data.

work differ somewhat from those obtained in Ref. 12. This is not unexpected, since the optical model affects both the inelastic partial widths, and, through the penetrabilities, the spectroscopic amplitudes obtained from these widths. It is evident from Table III that for slightly more than half of the spectroscopic amplitudes given, the agreement with theory is better for the present results than those in Ref. 12, while the reverse is true for only three cases.

Harney[24] pointed out that for reactions other than elastic scattering with spin $\frac{1}{2}$ particles, (1) if there is only a single partial wave in the entrance channel, the analyzing power will be zero for all exit channels, while polarization measurements will contain information on the exit-channel partial waves; (2) if there is only a single partial wave in an exit channel, the polarization in that channel will be zero while analyzing-power measurements in that channel will contain information on the entrance channel partial waves.

For protons incident on a spin-zero target with isolated resonances in the absence of direct amplitudes, there are sets of square roots of partial widths which give identical cross-section angular distributions,[25] since the expression for the cross section is quadratic in the root partial widths. For resonances with low spin, there are usually more inelastic partial widths than there are Legendre polynomial components in the cross-section angular distribution. In the case of resonances with spins other than $\frac{1}{2}$ (for which the cross section is isotropic and the polarization is zero), an angular distribution of polarization removes the ambiguity in the root partial widths and increases the amount of information available. In this context, the quality of the present polarization measurements is adequate for the extraction of useful information.

In this work with concurrent direct reaction amplitudes and thus a very large number of interfering partial waves in entrance and exit channels, angular distributions of polarization, analyzing power, and cross section for inelastic scattering are about equally sensitive to the resonant inelastic partial widths and contain essentially equivalent information. As an illustration of this point, Fig. 10 shows calculations for the $\frac{7}{2}^-$ resonance using the inelastic root partial widths from Table II with all combinations of phases for the $f_{7/2}$ and $p_{3/2}$ inelastic widths. The similarity of the inelastic angular distributions of polarization and analyzing power in Figs. 6, and 8—10 appears to be due in large measure to the strength of the direct reaction amplitudes rather than being only the result of a particular combination of resonance partial widths and phases. Similar calculations for the $\frac{3}{2}^-$ resonances show the same features.

The principal limitation on the polarimeter was that of analyzing detector count rate. With faster preamplifiers, pileup rejection, improved baseline restoration, detector cooling and overbiasing, and a thin target which is rotated to permit larger beam currents, it should be possible to have improved count-rate capabilities and better resolution. A factor of 10 improvement in efficiency is possible with a better geometry.[26]

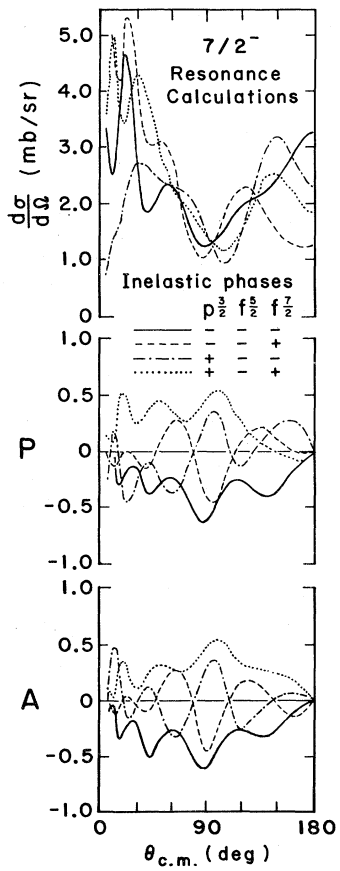

FIG. 10. Calculations of cross section, polarization, and analyzing power for inelastic scattering at the energy of the $\frac{7}{2}^-$ resonance using the absolute values of the square roots of inelastic partial widths from Table II. The solid line corresponds to the results of our analysis; the dashed line to a change in sign of the $p_{3/2}$ inelastic root partial width; the dot-dashed line to a change in sign of the $f_{7/2}$ inelastic root partial width; and the dotted line to a change in sign of both $f_{7/2}$ and $p_{3/2}$ inelastic root partial widths.

In summary, cross section and analyzing-power measurements combined with a coupled-channels-plus-resonance analysis have yielded optical model parameters which provide a better description of off-resonance cross section than the potential of Ref. 12 and at the same time describe analyzing-power data. Experimentally determined spectroscopic amplitudes for three analog states of the ^{130}Te-plus-proton system are in closer agreement with the particle vibrator calculation predictions of Ref. 12 than the experimental amplitudes from that work. For incident proton energies between 9 and 16 MeV and with the improvements discussed above, the back-angle silicon polarimeter can be a very useful device in situations where resolution is not critical and count rate in the analyzing detector not excessive.

*Present address: Ford Aerospace and Communications Corp, 1002 Gemini Avenue, Houston, TX 77058.

†Present address: Institut de Physique Nucleaires, F-91406 Orsay Cedex, France.

[1]S. Takeuchi, Y. Toba, and H. Sakaguchi, Nucl. Phys. **A288**, 251 (1977).

[2]S. Davis, C. Glashausser, A. B. Robbins, and G. Bissinger, Nucl. Phys. **A270**, 285 (1976).

[3]C. F. Haynes, S. Davis, C. Glashausser, and A. B. Robbins, Nucl. Phys. **A270**, 269 (1976).

[4]J. L. Foster, Jr., F. Krmpotić, and T. V. Ragland, Phys. Rev. C **17**, 1602 (1978).

[5]H. Clement and G. Graw, Phys. Lett. **57B**, 323 (1975).

[6]H. Clement, G. Graw, W. Kretschmer, and P. Schulze-Döbold, Phys. Rev. Lett. **27**, 526 (1971).

[7]R. N. Boyd *et al.*, Nucl. Phys. **A228**, 253 (1974).

[8]R. N. Boyd, S. Davis, C. Glashausser, and C. F. Haynes, Phys. Rev. Lett. **27**, 1590 (1971).

[9]P. Foissel, Y. Cassagnou, M. Laméhi-Rachti, C. Levi, W. Mittig, and L. Papineau, Nucl. Phys. **A178**, 640 (1971).

[10]G. Graw, H. Clement, J. H. Feist, W. Kretschmer, and P. Pröschel, Phys. Rev. C **10**, 2340 (1974).

[11]R. Arking, R. N. Boyd, J. C. Lombardi, A. B. Robbins, and S. Yoshida, Phys. Rev. Lett. **27**, 1396 (1971).

[12]M. C. Hermida M. Ruiz, M. L. Cescato, J. L. Foster, Jr., and F. Krmpotić, Phys. Rev. C **29**, 64 (1984).

[13]M. L. Cescato, M. C. Hermida, M. Ruiz, J. L. Foster, Jr., and F. Krmpotić, Phys. Rev. C **29**, 49 (1984).

[14]H. O. Meyer, W. G. Weitkamp, J. S. Dunham, T. A. Trainor, and M. P. Baker, Nucl. Phys. **A269**, 269 (1976), and references therein.

[15]H. R. Hiddleston, J. A. Aymar, and S. E. Darden, Nucl. Phys. **A242**, 323 (1975).

[16]J. P. Martin and R. J. A. Levesque, Nucl. Instrum. Methods **84**, 211 (1970).

[17]J. P. Martin, Ph.D. thesis, University of Montreal (unpublished).

[18]C. F. Williamson, J. P. Boujot, and J. Picard, Saclay Report CEA-R 3042, 1966.

[19]P. Depommier and J. Lequyer, program GENEVE, University of Montreal.

[20]J. Raynal, program ECIS 78, Saclay (private communication).

[21]W. J. Thompson, in *Nuclear Isospin,* edited by J. D. Anderson, S. R. Bloom, J. Cerny, and W. W. True (Academic, New York, 1970).

[22]J. Raynal, Saclay Centre d'Etudes Nucléaires report (unpublished).

[23]W. J. Thompson, J. L. Adams, and D. Robson, Phys. Rev. **173**, 975 (1968).

[24]H. L. Harney, Phys. Lett. **28B**, 249 (1968).

[25]J. L. Foster, Jr., O. Dietzsch, and L. Bimbot, Phys. Rev. Lett. **31**, 731 (1973).

[26]J. P. Martin, J. L. Foster, Jr., H. R. Hiddleston, and S. E. Darden, Nucl. Instrum. Methods **113**, 477 (1973).